International Journal of Control, Automation and Systems 20(6) (2022) 1757-1771
http://dx.doi.org/10.1007/s12555-021-0267-x
ISSN:1598-6446 eISSN:2005-4092
http://www.springer.com/12555

Optimal Zonotopic Kalman Filter-based State Estimation and Fault-diagnosis Algorithm for Linear Discrete-time System with Time Delay

Zi-Xing Liu, Zi-Yun Wang*, Yan Wang, and Zhi-Cheng Ji

Abstract: To manage the state estimation and fault-diagnosis problem of linear discrete uncertain systems with time delay, a state estimation and fault-diagnosis algorithm based on an improved zonotopic Kalman filter is proposed under the assumption that the process interference and measurement noise of the systems are unknown but bounded. First, zonotopes are used to contain the nonzero initial conditions of the system with time delay, and an optimal zonotopic Kalman filter is designed by using an iterative replacement method to determine the relationship between the current time and the delayed time. Subsequently, the optimal observer gain of the optimal zonotopic Kalman filter is designed by minimizing the size of the zonotopic sets to estimate the state sets. Next, the fault occurrence is detected by determining whether the true output value of the system is within the upper and lower bounds of the estimated output value, and the fault identification process is completed by the matching probability of the fault type. Finally, the fault-diagnosis of a numerical system, and the pitch system of a wind turbine are used as examples to demonstrate the effectiveness and feasibility of the proposed method for systems with time delay by analyzing the fault diagnosis results. A comparison with a normal fault-matching method indicates that the proposed fault-diagnosis algorithm is more rapid in fault identification.

Keywords: Fault diagnosis, linear system, state estimation, time delay, zonotopic Kalman filter.

1. INTRODUCTION

System operational safety and product quality are important for industrial process control, and its failure will decrease quality and create severe safety risks to the entire system. Therefore, the study of fault detection and diagnosis is significant [1]. Researchers in the related fields have divided the fault-diagnosis methods into the following three categories: analytical model-based [2–4], knowledge-based [5,6], and signal-processing-based [7, 8]. Furthermore, in order to maintain the good performance of the system, a variety of effective fault-tolerant control methods have been proposed and developed [9, 10]. Among the three fault-diagnosis methods mentioned above, the analytical model-based method having a solid theoretical foundation is currently a popular research topic owing to its simple implementation.

However, traditional model-based methods assume that noise and interference conform to a certain distribution law; but actual systems contain insufficient data to summarize the random characteristics of these noises. Furthermore, certain noises do not have random characteristics, making it difficult to describe using statistical rules. If these methods are applied to solve the fault-diagnosis problem of an actual system, they may result in false or missed detections. Therefore, the shortcomings of these methods limit their practical applications. In contrast to these fault-diagnosis methods, such as the Kalman filter [11] and recursive least square algorithm [12], which are used to manage systems whose interference and noise are unbounded but satisfy certain distribution laws, the set-membership estimation method only requires knowledge of the interference and noise bounds; thus, it can be used to solve the aforementioned problems effectively and can be satisfied for most metropolitan systems. Therefore, the set-membership estimation method has been extensively studied and widely used. The fault-diagnosis method based on set-membership estimation can be divided into the following two categories: parameter set estimation-based [13,14] and state set estimation-based [15–17]. As implied by the names, the fault-diagnosis method based on parameter set estimation obtains the

Manuscript received March 31, 2021; revised June 22, 2021; accepted August 13, 2021. Recommended by Associate Editor Zehui Mao under the direction of Editor Bin Jiang. This work is supported in part by the the National Key Research and Development Program of China (2020YFB1710600), the Jiangsu Science and Technology Association Young Science and Technology Talents Lifting Project (TJ-2021-006) and the National Natural Science Foundation of China (61973138).

Zi-Xing Liu and Zi-Yun Wang are with the Key Laboratory of Advanced Process Control for Light Industry, Ministry of Education, Jiangnan University, Jiangsu, China (e-mails: {hsjnlzx, wangzy0601}@163.com). Yan Wang and Zhi-Cheng Ji are with the Engineering Research Center of Internet of Things Technology and Applications, Ministry of Education, Jiangnan University, Jiangsu, China (e-mails: yanwangjn@163.com, zcji@jiangnan.edu.cn).
* Corresponding author.

fault diagnosis result of the system according to the obtained parameter set, whereas the fault-diagnosis method based on state set estimation determines the fault state of the system based on the corresponding state set. The two methods are not superior to each other. The following set-membership filtering methods are commonly used ellipsoids [18,19], zonotopes [15,16,20], and polytopes [21,22]; the zonotopes have better accuracy, are less conservative than ellipsoids, and are lower in complexity compared to polytopes [23].

The zonotopic Kalman filter (ZKF) [24] is a state estimation algorithm that combines a zonotopic set and a Kalman filter. By obtaining the optimal observer gain, a ZKF is designed to estimate the state set, and the zonotopic set is used to describe the state of the system with an unknown but bounded interference and noise. Zhang *et al.* [25] designed a ZKF based on the construction of an augmented system for systems with a sensor fault to determine its interval estimation, and the simulation results of a quadruple-tank system demonstrated the effectiveness and superiority of the proposed method. Pourasghar *et al.* [26] proposed a zonotopic Kalman filter based fault detection method (FD-ZKF) based on the ZKF algorithm for the fault detection of a system to enhance the sensitivity to faults with respect to disturbances. The simulation of the quadruple-tank system illustrates the effectiveness of the proposed FD-ZKF method.

Time delay widely exists in various practical systems, which will lead to poor performance or system instability. There are many reasons for time delay, such as time delay in measurement caused by aging of system components and time delay in signal transmission caused by mechanical wear [27,28]. For a system with time delay, except for the actuator input item and process interference item, the current real state is not only related to the state at the previous time, but also related to the state several time ago due to the time delay. Therefore, when calculating the estimated value of the current state, not only the state estimation result at the previous moment needs to be considered, but also the influence of the state estimation result several time ago needs to be added. Thus, compared to the simple calculation of the state estimation result at the previous time, the calculation of the system with time delay is more complicated and more suitable for the actual situation. Therefore, the research and control of systems with time delay have recently become popular in the field of control [29,30]. Considering a situation where the control performance of the time delay DC motor system would be significantly deteriorated under uncertain time delay information, Yook *et al.* [31] proposed a speed control problem for the time delay DC motor system. A predicted output signal was generated by incorporating a disturbance observer and a communication disturbance observer; comparative simulations and experiments tested the effectiveness of the proposed algorithm. Zhang *et al.* [32] proposed a novel reachable set estimation method based on zonotopes for the linear discrete-time system with time delay, and three numerical simulations demonstrated the effectiveness of the proposed method. To solve the sensor fault-diagnosis problems of time-delay nonlinear systems, You *et al.* [33] presented a sensor fault-diagnosis approach via the use of adaptive updating rules; the simulation examples prove the effectiveness of the proposed algorithm, which can track the fault signal effectively.

Based on the universality of the system with time delay and the superiority of the ZKF method, this study investigates the state estimation and fault diagnosis of a linear discrete-time system with time delay by designing an optimal ZKF algorithm to obtain accurate state estimation results. A zonotope is used to describe the estimated state set subject to an unknown but bounded noise, and the state estimation results were used for subsequent fault diagnosis. The fault-matching method is a commonly used fault identification method, which identifies system faults through the matching degree between the fault model and the actual model [34]. Based on this, the fault-matching method combined with the Bayesian theory is used in this study to complete the fault identification using the matching probability of the fault type. A comparison of the two identification methods demonstrates that the normal fault-matching method has lower efficiency.

The main contributions of this study are as follows: 1) Considering the influence of time delay on the system, an iterative replacement method is used to determine the relationship between the current time and the delayed time, and an optimal ZKF is designed. 2) An optimal gain matrix is calculated for the optimal zonotopic Kalman filter by minimizing the size of the zonotopic set corresponding to the state of the system with time delay. 3) The fault-matching method combined with the Bayesian theory is used for fault identification; that is, the fault identification process is completed through the matching probability of the fault type. Compared to the normal fault-matching method, the proposed fault-matching method is more rapid in fault identification.

The rest of this paper is organized as follows: Section 2 presents the problem formulation and preliminaries. The design of the optimal ZKF method with time delay is demonstrated in Section 3. Section 4 derives the fault-diagnosis method. In Section 5, a numerical simulation case and a pitch system of a wind turbine simulation case are used to verify and explain the effectiveness of the proposed fault-diagnosis method for a system with time delay. Finally, Section 6 presents a brief conclusion of the proposed algorithm.

2. PROBLEM FORMULATION AND PRELIMINARIES

Considering the following linear discrete uncertain system with time delay:

$$\begin{cases} x(k+1) = Ax(k) + A_h x(k-h) + Bu(k) + Dw(k), \\ y(k) = Cx(k) + Fv(k), \end{cases} \tag{1}$$

where $x(k) \in \mathbb{R}^{n_x}$, $u(k) \in \mathbb{R}^{n_u}$, and $y(k) \in \mathbb{R}^{n_y}$ are the state, input, and measurement output vectors of the system at time k, respectively; A, A_h, B, D, C, and F are parameter matrices of the appropriate dimensions, $h \in \mathbb{Z}_+$ denotes a known constant time delay, and $w(k) \in \mathbb{R}^{n_w}$ and $v(k) \in \mathbb{R}^{n_v}$ are the unknown but bounded process interference and measurement noise of the system, respectively.

The essential definitions and properties presented in this study are as follows:

Definition 1: The r-order zonotope $\mathcal{Z} \subset \mathbb{R}^n$, $(n \le r)$ is defined as follows [25]:

$$\begin{aligned} \mathcal{Z} &= p \oplus G\boldsymbol{B}^r \\ &= \{z \in \mathbb{R}^n : z = p + Gb, b \in \boldsymbol{B}^r\} = \langle p, G \rangle, \end{aligned} \tag{2}$$

where $\boldsymbol{B}^r = [-1, 1]^r$ is a hypercube, $p \in \mathbb{R}^n$ is the center of $\mathcal{Z}$, and $G \in \mathbb{R}^{n \times r}$ is the generator matrix that is used to define the shape of $\mathcal{Z}$.

Zonotope is a special class of the geometrical sets and has the following certain computational properties:

Property 1: For two zonotopes $\mathcal{Z}_1 = \langle p_1, G_1 \rangle \subset \mathbb{R}^n$ and $\mathcal{Z}_2 = \langle p_2, G_2 \rangle \subset \mathbb{R}^n$, the Minkowski sum is also a zonotope, and can be defined as follows [25]:

$$\langle p_1, G_1 \rangle \oplus \langle p_2, G_2 \rangle = \langle p_1 + p_2, [G_1 \; G_2] \rangle. \tag{3}$$

Property 2: The linear image of the zonotope $\mathcal{Z} = \langle p, G \rangle \subset \mathbb{R}^n$ by $L \in \mathbb{R}^{l \times n}$ is computed using the following matrix product [25]:

$$L \odot \langle p, G \rangle = \langle Lp, LG \rangle. \tag{4}$$

Property 3: The smallest interval hull $\mathrm{Box}(\mathcal{Z}) = [z^-, z^+] = \{z : z \in \mathcal{Z}, z^- \le z \le z^+\}$ containing the zonotope $\mathcal{Z} = \langle p, G \rangle \subset \mathbb{R}^n$ can be described as follows [25]:

$$\begin{cases} z_i^- = p_i - \sum_{j=1}^{r} |G_{i,j}|, \;\; i = 1, \cdots, n, \\ z_i^+ = p_i + \sum_{j=1}^{r} |G_{i,j}|, \;\; i = 1, \cdots, n, \end{cases} \tag{5}$$

where z_i^-, z_i^+, and p_i are the ith components of z^-, z^+, and p, respectively. According to the aforementioned definitions, the interval hull of $\mathcal{Z}$ can also be expressed as $\langle p, rs(G) \rangle$, where $rs(G)$ is a diagonal matrix and $rs(G)_{ij} = \sum_{j=1}^{r} |G_{i,j}|$, $i = 1, \cdots, n$.

Lemma 1: The reduction operator $\downarrow_s$ can be used to simplify the zonotopes. For a zonotope $\mathcal{Z} = p \oplus GB^r \subset \mathbb{R}^n$, $(n \le s \le r)$, it can be bounded by a more conservative zonotope with lower dimensions as follows [24]:

$$\mathcal{Z} = \langle p, G \rangle \subseteq \langle p, \downarrow_s G \rangle. \tag{6}$$

Thus, the implement procedure of $\downarrow_s G$ can be summarized as follows:

- Obtain the norm decreasing matrix $\downarrow G$ by rearranging the columns in the matrix G in decreasing Euclidean norm order as follows:

$$\begin{aligned} &\downarrow G = [g_1, \, g_2, \, \cdots, \, g_r], \\ &\quad \|g_j\|_2 \ge \|g_{j+1}\|_2, \;\; j = 1, \, \cdots, \, r-1. \end{aligned}$$

- Divide $\downarrow G$ into two parts, $G_>$ and $G_<$, and replace $G_<$ by a diagonal matrix $rs(G_<) \in \mathbb{R}^{n \times n}$ as follows:
  If $r \le s$ **then** $\downarrow_s G = \downarrow G$.
  Else $\downarrow_s G = [G_>, rs(G_<)] \in \mathbb{R}^{n \times s}$, $G_> = [g_1, \cdots, g_{s-n}]$, and $G_< = [g_{s-n+1}, \cdots, g_r]$.

Definition 2: The Frobenius radius of the zonotope $\mathcal{Z} = \langle p, G \rangle$ can be regarded as a size criterion of the zonotope, and can be defined as the Frobenius norm of G [24]

$$\|\langle p, G \rangle\|_F = \|G\|_F = \sqrt{tr(G^{\mathrm{T}}G)} = \sqrt{tr(GG^{\mathrm{T}})}. \tag{7}$$

Similarly, in the weighted case, $\|G\|_{F,M} = \sqrt{tr(G^{\mathrm{T}}MG)}$, where $M \in \mathbb{R}^{n \times n}$ is a weighted symmetric positive definite matrix, $tr(\cdot)$ is the trace of a matrix.

Definition 3: The covariation of a zonotope $\mathcal{Z} = \langle p, G \rangle$ is defined as $cov(\langle p, G \rangle) = GG^{\mathrm{T}}$ [24]. The Frobenius radius minimization is equivalent to its covariation trace minimization, so $J = tr(GG^{\mathrm{T}}) = \|G\|_F^2$ can also be the size criterion of the zonotope $\mathcal{Z} = \langle p, G \rangle$, and $J_M = tr(MGG^{\mathrm{T}}) = tr(G^{\mathrm{T}}MG) = \|G\|_{F,M}^2$ in the weighted case.

Definition 4: Certain correlation operations about the matrix traces are as follows [24,35]:

$$tr(A) = tr(A^{\mathrm{T}}), \tag{8}$$

$$tr(AB) = tr(BA), \tag{9}$$

$$\frac{\partial tr(AX^{\mathrm{T}}B)}{\partial X} = A^{\mathrm{T}}B^{\mathrm{T}}, \tag{10}$$

$$\frac{\partial tr(AXBX^{\mathrm{T}}C)}{\partial X} = BX^{\mathrm{T}}CA + B^{\mathrm{T}}X^{\mathrm{T}}A^{\mathrm{T}}C^{\mathrm{T}}, \tag{11}$$

where A, B, C, and X are matrices with appropriate dimensions.

Assumption 1: The initial state, process interference, and measurement noise of the system (1) are confined to the zonotopic sets as follows:

$$\begin{aligned} &x(k-h) \in X(k-h) = \langle p(k-h), G(k-h) \rangle, \\ &0 \leqslant k \leqslant h, \end{aligned} \tag{12}$$

$$w(k) \in W = \langle 0,\ G_w \rangle,\ k \geqslant 0, \tag{13}$$
$$v(k) \in V = \langle 0,\ G_v \rangle,\ k \geqslant 0, \tag{14}$$

where $p(k-h) \in \mathbb{R}^{n_x}$, $G(k-h) \in \mathbb{R}^{n_x \times n_x}$, $G_w \in \mathbb{R}^{n_w \times n_w}$, and $G_v \in \mathbb{R}^{n_v \times n_v}$ are known constant vector and matrices.

3. DESIGN OF THE OPTIMAL ZKF FOR THE SYSTEM WITH TIME DELAY

The fault diagnosis for the system with time delay is based on the estimated states, and the states contained in the zonotopic sets are estimated by designing an optimal ZKF.

For system (1), the design of the optimal ZKF is as follows:

$$\begin{aligned}\hat{x}(k+1) = {} & A\hat{x}(k) + A_h\hat{x}(k-h) + Bu(k) + Dw(k) \\ & + L(k)(y(k) - C\hat{x}(k) - Fv(k)),\end{aligned} \tag{15}$$

where $L(k)$ is the estimated optimal gain matrix of the optimal ZKF, and $\hat{x}(k)$ represents the estimated state at time k.

Theorem 1: The estimated state at time $k+1$ can be contained in the zonotopic set as follows when $0 \leqslant k \leqslant h$:

$$\hat{x}(k+1) \in \hat{X}(k+1) = \langle \hat{p}(k+1), \hat{G}(k+1) \rangle, \tag{16}$$

where

$$\begin{aligned}\hat{p}(k+1) = {} & (A - L(k)C)\hat{p}(k) + A_h\hat{p}(k-h) \\ & + Bu(k) + L(k)y(k),\end{aligned} \tag{17}$$
$$\begin{aligned}\hat{G}(k+1) = {} & [(A - L(k)C)\tilde{\hat{G}}(k) \quad A_h\tilde{\hat{G}}(k-h) \\ & DG_w \quad -L(k)FG_v],\end{aligned} \tag{18}$$
$$\tilde{\hat{G}}(k) = \downarrow_s \hat{G}(k),\ \tilde{\hat{G}}(k-h) = \downarrow_s \hat{G}(k-h), \tag{19}$$
$$\hat{p}(k-h) = p(k-h),\ 0 \leqslant k \leqslant h, \tag{20}$$
$$\hat{G}(k-h) = G(k-h),\ 0 \leqslant k \leqslant h. \tag{21}$$

Proof: According to the description of system (1), the time delay only depends on the initial condition when $0 \leqslant k \leqslant h$. Based on (15), and the properties of the zonotope, we can obtain the following:

$$\begin{aligned}&\hat{x}(k+1) \\ &= A\hat{x}(k) + A_h\hat{x}(k-h) + Bu(k) + Dw(k) \\ &\quad + L(k)(y(k) - C\hat{x}(k) - Fv(k)) \\ &\in \big((A - L(k)C) \odot \langle \hat{p}(k), \hat{G}(k) \rangle\big) \\ &\quad \oplus (A_h \odot \langle \hat{p}(k-h), \hat{G}(k-h) \rangle) \oplus Bu(k) \\ &\quad \oplus (D \odot \langle 0, G_w \rangle) \oplus L(k)y(k) \oplus (-L(k)F \odot \langle 0, G_v \rangle) \\ &\subseteq \langle (A - L(k)C)\hat{p}(k) + A_h\hat{p}(k-h) + Bu(k) + L(k)y(k), \\ &\quad [(A - L(k)C)\tilde{\hat{G}}(k) \ \ A_h\tilde{\hat{G}}(k-h) \\ &\quad DG_w \ \ -L(k)FG_v] \rangle,\end{aligned} \tag{22}$$

where $\tilde{\hat{G}}(k) = \downarrow_s \hat{G}(k)$ and $\tilde{\hat{G}}(k-h) = \downarrow_s \hat{G}(k-h)$ are the complexity reduction matrices of $\hat{G}(k)$ and $\hat{G}(k-h)$, respectively. □

Theorem 2: For the zonotopic set in (16), we define $\tilde{P}(k) = \tilde{\hat{G}}(k)\tilde{\hat{G}}^{\mathrm{T}}(k)$, $Q_v = FG_vG_v^{\mathrm{T}}F^{\mathrm{T}}$. Then, the optimal gain matrix $L(k)$ can be designed as follows:

$$L(k) = AK(k), \tag{23}$$
$$K(k) = R(k)S^{-1}(k), \tag{24}$$
$$R(k) = \tilde{P}(k)C^{\mathrm{T}}, \tag{25}$$
$$S(k) = C\tilde{P}(k)C^{\mathrm{T}} + Q_v. \tag{26}$$

Proof: $J_M(k+1) = tr(\hat{G}^{\mathrm{T}}(k+1)M\hat{G}(k+1))$ is the index that determines the size of the zonotope $\hat{X}(k+1)$, and the optimal value of $L(k)$ can be obtained such that $\partial_{L(k)}J_M(k+1) = 0$.

$$\begin{aligned}&\partial_{L(k)}J_M(k+1) \\ &= \partial_{L(k)}tr(\hat{G}^{\mathrm{T}}(k+1)M\hat{G}(k+1)) \\ &= \partial_{L(k)}tr\big(M(A - L(k)C)\tilde{P}(k)(A - L(k)C)^{\mathrm{T}} \\ &\quad + M\tilde{P}_h(k-h) + MQ_w + ML(k)Q_vL^{\mathrm{T}}(k)\big) \\ &= \partial_{L(k)}tr\big(M(L(k)C\tilde{P}(k)C^{\mathrm{T}}L^{\mathrm{T}}(k) + L(k)Q_vL^{\mathrm{T}}(k))\big) \\ &\quad - 2\partial_{L(k)}tr(MA\tilde{P}(k)C^{\mathrm{T}}L^{\mathrm{T}}(k)).\end{aligned} \tag{27}$$

Let $\partial_{L(k)}J_M(k+1) = 0$, then

$$\begin{aligned}&\partial_{L(k)}tr\big(M(L(k)C\tilde{P}(k)C^{\mathrm{T}}L^{\mathrm{T}}(k) + L(k)Q_vL^{\mathrm{T}}(k))\big) \\ &= 2\partial_{L(k)}tr(MA\tilde{P}(k)C^{\mathrm{T}}L^{\mathrm{T}}(k)).\end{aligned} \tag{28}$$

Considering the operations of the matrix traces and $M = M^{\mathrm{T}} > 0$, we can obtain the following:

$$L(k)(C\tilde{P}(k)C^{\mathrm{T}} + Q_v) = A\tilde{P}(k)C^{\mathrm{T}}, \tag{29}$$
$$L(k)S(k) = AR(k), \tag{30}$$
$$L(k) = AK(k), \tag{31}$$

where $K(k) = R(k)S^{-1}(k)$, $R(k) = \tilde{P}(k)C^{\mathrm{T}}$, $S(k) = C\tilde{P}(k)C^{\mathrm{T}} + Q_v$, $\tilde{P}(k) = \tilde{\hat{G}}(k)\tilde{\hat{G}}^{\mathrm{T}}(k)$, $\tilde{P}_h(k-h) = A_h\tilde{\hat{G}}(k-h)\tilde{\hat{G}}^{\mathrm{T}}(k-h)A_h^{\mathrm{T}}$, $Q_w = DG_wG_w^{\mathrm{T}}D^{\mathrm{T}}$, $Q_v = FG_vG_v^{\mathrm{T}}F^{\mathrm{T}}$. □

Theorem 3: The estimated state at time $k+1$ can be contained in the zonotopic set as follows when $k > h$:

$$\hat{x}(k+1) \in \hat{X}(k+1) = \langle \hat{p}(k+1), \hat{G}(k+1) \rangle, \tag{32}$$

where

$$\begin{aligned}&\hat{p}(k+1) \\ &= \Big((A - L(k)C)\prod_{i=1}^{h}(A - L(k-i)C) + A_h\Big) \\ &\quad \times \hat{p}(k-h) + (A - L(k)C)\end{aligned}$$

$$\times\sum_{i=1}^{h}\Big(\prod_{j=1}^{i-1}(A-L(k-j)C)A_h\hat{p}(k-h-i)\Big)$$
$$+(A-L(k)C)\sum_{i=1}^{h}\Big(\prod_{j=1}^{i-1}(A-L(k-j)C)(Bu(k-i)$$
$$+L(k-i)y(k-i))\Big)+Bu(k)+L(k)y(k), \quad (33)$$

$$\hat{G}(k+1)$$
$$=\Big[\Big((A-L(k)C)\prod_{i=1}^{h}(A-L(k-i)C)+A_h\Big)\tilde{\tilde{G}}(k-h)$$
$$H_1(k)\quad H_2(k)\quad H_3(k)\Big], \quad (34)$$

$$H_1(k)=[H_{11}(k)\quad H_{12}(k)\quad\cdots\quad H_{1h}(k)], \quad (35)$$

$$H_{1i}(k)=(A-L(k)C)$$
$$\times\prod_{j=1}^{i-1}(A-L(k-j)C)A_h\tilde{\tilde{G}}(k-h-i), \quad (36)$$

$$H_2(k)=[H_{21}(k)\,H_{22}(k)\,\cdots\,H_{2h}(k)\,DG_w], \quad (37)$$

$$H_{2i}(k)=(A-L(k)C)\prod_{j=1}^{i-1}(A-L(k-j)C)DG_w, \quad (38)$$

$$H_3(k)=[H_{31}(k)\,H_{32}(k)\,\cdots\,H_{3h}(k)\,-L(k)FG_v], \quad (39)$$

$$H_{3i}(k)=-(A-L(k)C)$$
$$\times\prod_{j=1}^{i-1}(A-L(k-j)C)\cdot L(k-i)FG_v, \quad (40)$$

and $\tilde{\tilde{G}}(k-h)=\downarrow_s\hat{G}(k-h)$, $\tilde{\tilde{G}}(k-h-i)=\downarrow_s\hat{G}(k-h-i)$, $\hat{G}(k+1)\in\mathbb{R}^{n_x\times(r+n_{H_1}+n_{H_2}+n_{H_3})}$, $H_1(k)\in\mathbb{R}^{n_x\times n_{H_1}}$, $H_2(k)\in\mathbb{R}^{n_x\times n_{H_2}}$, $H_3(k)\in\mathbb{R}^{n_x\times n_{H_3}}$.

Proof: The time delay of the system (1) is related to the operation of the system when $k>h$, thus the influence of the time delay on the state estimation of the system at time $k+1$ should be considered. The relationship between $x(k)$ and $x(k-h)$ is considered, and the state of the system is iterated from $x(k-h)$ to $x(k+1)$.

When $k>h$, we can obtain the following from (15):

$$\hat{x}(k+1)=(A-L(k)C)\hat{x}(k)+A_h\hat{x}(k-h)+Bu(k)$$
$$+Dw(k)+L(k)y(k)-L(k)Fv(k), \quad (41)$$
$$\vdots\qquad\qquad\vdots$$
$$\hat{x}(k-i)=(A-L(k-1-i)C)\hat{x}(k-1-i)$$
$$+A_h\hat{x}(k-h-1-i)+Bu(k-1-i)$$
$$+Dw(k-1-i)+L(k-1-i)y(k-1-i)$$
$$-L(k-1-i)Fv(k-1-i), \quad (42)$$
$$\vdots\qquad\qquad\vdots$$
$$\hat{x}(k-h)=(A-L(k-1-h)C)\hat{x}(k-1-h)$$
$$+A_h\hat{x}(k-h-1-h)+Bu(k-1-h)$$
$$+Dw(k-1-h)+L(k-1-h)y(k-1-h)$$
$$-L(k-1-h)Fv(k-1-h). \quad (43)$$

Thus,

$$\hat{x}(k+1)$$
$$=(A-L(k)C)\hat{x}(k)+A_h\hat{x}(k-h)+Bu(k)+Dw(k)$$
$$+L(k)y(k)-L(k)Fv(k)$$
$$=(A-L(k)C)(A-L(k-1)C)\hat{x}(k-1)$$
$$+A_h\hat{x}(k-h)+(A-L(k)C)A_h\hat{x}(k-h-1)$$
$$+Bu(k)+(A-L(k)C)Bu(k-1)+Dw(k)$$
$$+(A-L(k)C)Dw(k-1)+L(k)y(k)$$
$$+(A-L(k)C)L(k-1)y(k-1)-L(k)Fv(k)$$
$$-(A-L(k)C)L(k-1)Fv(k-1)$$
$$\vdots\qquad\qquad\vdots$$
$$=\Big((A-L(k)C)\prod_{i=1}^{h}(A-L(k-i)C)+A_h\Big)\hat{x}(k-h)$$
$$+(A-L(k)C)$$
$$\times\sum_{i=1}^{h}\Big(\prod_{j=1}^{i-1}(A-L(k-j)C)A_h\hat{x}(k-h-i)\Big)$$
$$+(A-L(k)C)\sum_{i=1}^{h}\Big(\prod_{j=1}^{i-1}(A-L(k-j)C)(Bu(k-i)$$
$$+Dw(k-i)+L(k-i)y(k-i)$$
$$-L(k-i)Fv(k-i))\Big)$$
$$+Bu(k)+Dw(k)+L(k)y(k)-L(k)Fv(k)$$
$$\subseteq\Big\langle\Big((A-L(k)C)\prod_{i=1}^{h}(A-L(k-i)C)+A_h\Big)\hat{p}(k-h)$$
$$+(A-L(k)C)$$
$$\times\sum_{i=1}^{h}\Big(\prod_{j=1}^{i-1}(A-L(k-j)C)A_h\hat{p}(k-h-i)\Big)$$
$$+(A-L(k)C)\sum_{i=1}^{h}\Big(\prod_{j=1}^{i-1}(A-L(k-j)C)$$
$$\times(Bu(k-i)+L(k-i)y(k-i))\Big)+Bu(k)$$
$$+L(k)y(k),\ \Big[\Big((A-L(k)C)\prod_{i=1}^{h}(A-L(k-i)C)$$
$$+A_h\Big)\tilde{\tilde{G}}(k-h\quad H_1(k)\quad H_2(k)\quad H_3(k)\Big]\Big\rangle$$
$$=\langle\hat{p}(k+1),\hat{G}(k+1)\rangle, \quad (44)$$

where

$$H_1(k)=[H_{11}(k)\quad H_{12}(k)\quad\cdots\quad H_{1h}(k)], \quad (45)$$

$$H_{1i}(k)=(A-L(k)C)\prod_{j=1}^{i-1}(A-L(k-j)C)A_h$$
$$\times\tilde{\tilde{G}}(k-h-i), \quad (46)$$

$$H_2(k)=[H_{21}(k)\,H_{22}(k)\,\cdots\,H_{2h}(k)\,DG_w], \quad (47)$$

$$H_{2i}(k)=(A-L(k)C)\prod_{j=1}^{i-1}(A-L(k-j)C)DG_w, \quad (48)$$

$$H_3(k)=[H_{31}(k)\,H_{32}(k)\,\cdots\,H_{3h}(k)\,-L(k)FG_v], \tag{49}$$

$$H_{3i}(k)=-(A-L(k)C)\prod_{j=1}^{i-1}(A-L(k-j)C)\times L(k-i)FG_v, \tag{50}$$

and $\tilde{\hat{G}}(k-h)=\downarrow_s \hat{G}(k-h)$ and $\tilde{\hat{G}}(k-h-i)=\downarrow_s \hat{G}(k-h-i)$ are the complexity reduction matrices of $\hat{G}(k-h)$ and $\hat{G}(k-h-i)$, respectively, $\hat{G}(k+1)\in\mathbb{R}^{n_x\times(r+n_{H_1}+n_{H_2}+n_{H_3})}$, $H_1(k)\in\mathbb{R}^{n_x\times n_{H_1}}$, $H_2(k)\in\mathbb{R}^{n_x\times n_{H_2}}$, $H_3(k)\in\mathbb{R}^{n_x\times n_{H_3}}$. □

Theorem 4: For the zonotopic set of (32), define

$$\tilde{P}(k)=\Big(\prod_{i=1}^{h}(A-L(k-i)C)\Big)\tilde{\hat{G}}(k-h)\tilde{\hat{G}}^{\mathrm{T}}(k-h)\times\Big(\prod_{i=1}^{h}(A-L(k-i)C)\Big)^{\mathrm{T}}, \tag{51}$$

$$\tilde{P}_{1i}(k)=\Big(\prod_{j=1}^{i-1}(A-L(k-j)C)\Big)A_h\tilde{\hat{G}}(k-h-i)\times\tilde{\hat{G}}^{\mathrm{T}}(k-h-i)A_h^{\mathrm{T}}\Big(\prod_{j=1}^{i-1}(A-L(k-j)C)\Big)^{\mathrm{T}}, \tag{52}$$

$$\tilde{P}_{2i}(k)=\Big(\prod_{j=1}^{i-1}(A-L(k-j)C)\Big)DG_wG_w^{\mathrm{T}}D^{\mathrm{T}}\times\Big(\prod_{j=1}^{i-1}(A-L(k-j)C)\Big)^{\mathrm{T}}, \tag{53}$$

$$\tilde{P}_{3i}(k)=\Big(\prod_{j=1}^{i-1}(A-L(k-j)C)\Big)L(k-i)FG_vG_v^{\mathrm{T}}F^{\mathrm{T}}\times L^{\mathrm{T}}(k-i)\Big(\prod_{j=1}^{i-1}(A-L(k-j)C)\Big)^{\mathrm{T}}, \tag{54}$$

$$Q_v=FG_vG_v^{\mathrm{T}}F^{\mathrm{T}}. \tag{55}$$

The optimal gain matrix $L(k)$ can be designed as follows:

$$L(k)=AK_1(k)+A_hK_2(k), \tag{56}$$

$$K_1(k)=R_1(k)S^{-1}(k), \tag{57}$$

$$K_2(k)=R_2(k)S^{-1}(k), \tag{58}$$

$$R_1(k)=\Big(\tilde{P}(k)+\sum_{i=1}^{h}(\tilde{P}_{1i}(k)+\tilde{P}_{2i}(k)+\tilde{P}_{3i}(k))\Big)C^{\mathrm{T}}, \tag{59}$$

$$R_2(k)=A_h\tilde{\hat{G}}(k-h)\tilde{\hat{G}}^{\mathrm{T}}(k-h)\times\Big(\prod_{i=1}^{h}(A-L(k-i)C)\Big)^{\mathrm{T}}C^{\mathrm{T}}, \tag{60}$$

$$S(k)=C\Big(\tilde{P}(k)+\sum_{i=1}^{h}(\tilde{P}_{1i}(k)+\tilde{P}_{2i}(k)+\tilde{P}_{3i}(k))\Big)C^{\mathrm{T}}+Q_v. \tag{61}$$

Proof: $L(k)$ is obtained by minimizing $J_M(k+1)=tr(\hat{G}^{\mathrm{T}}(k+1)M\hat{G}(k+1))$. Thus,

$$\begin{aligned}
&\partial_{L(k)}J_M(k+1)\\
&=\partial_{L(k)}tr(\hat{G}^{\mathrm{T}}(k+1)M\hat{G}(k+1))\\
&=\partial_{L(k)}tr\Big(ML(k)C\tilde{P}(k)C^{\mathrm{T}}L^{\mathrm{T}}(k)-2MA\tilde{P}(k)C^{\mathrm{T}}L^{\mathrm{T}}(k)\Big)\\
&\quad-2\partial_{L(k)}tr\Big(MA_h\tilde{\hat{G}}(k-h)\tilde{\hat{G}}^{\mathrm{T}}(k-h)\times\Big(\prod_{i=1}^{h}(A-L(k-i)C)\Big)^{\mathrm{T}}C^{\mathrm{T}}L^{\mathrm{T}}(k)\Big)\\
&\quad+\partial_{L(k)}tr\Big(M\sum_{i=1}^{h}(L(k)C\tilde{P}_{1i}(k)C^{\mathrm{T}}L^{\mathrm{T}}(k))-2M\sum_{i=1}^{h}(A\tilde{P}_{1i}(k)C^{\mathrm{T}}L^{\mathrm{T}}(k))\Big)\\
&\quad+\partial_{L(k)}tr\Big(M\sum_{i=1}^{h}(L(k)C\tilde{P}_{2i}(k)C^{\mathrm{T}}L^{\mathrm{T}}(k))-2M\sum_{i=1}^{h}(A\tilde{P}_{2i}(k)C^{\mathrm{T}}L^{\mathrm{T}}(k))\Big)\\
&\quad+\partial_{L(k)}tr\Big(M\sum_{i=1}^{h}(L(k)C\tilde{P}_{3i}(k)C^{\mathrm{T}}L^{\mathrm{T}}(k))-2M\sum_{i=1}^{h}(A\tilde{P}_{3i}(k)C^{\mathrm{T}}L^{\mathrm{T}}(k))+ML(k)Q_vL^{\mathrm{T}}(k)\Big).
\end{aligned} \tag{62}$$

Let $\partial_{L(k)}J_M(k+1)=0$, then

$$\begin{aligned}
&\partial_{L(k)}tr\Big(ML(k)C\Big(\tilde{P}(k)+\sum_{i=1}^{h}(\tilde{P}_{1i}(k)+\tilde{P}_{2i}(k)+\tilde{P}_{3i}(k))\Big)\times C^{\mathrm{T}}L^{\mathrm{T}}(k)+ML(k)Q_vL^{\mathrm{T}}(k)\Big)\\
&=2\partial_{L(k)}tr\Big(MA\Big(\tilde{P}(k)+\sum_{i=1}^{h}(\tilde{P}_{1i}(k)+\tilde{P}_{2i}(k)+\tilde{P}_{3i}(k))\Big)\times C^{\mathrm{T}}L^{\mathrm{T}}(k)\Big)+2\partial_{L(k)}tr\Big(MA_h\tilde{\hat{G}}(k-h)\tilde{\hat{G}}^{\mathrm{T}}(k-h)\\
&\quad\times\Big(\prod_{i=1}^{h}(A-L(k-i)C)\Big)^{\mathrm{T}}C^{\mathrm{T}}L^{\mathrm{T}}(k)\Big).
\end{aligned} \tag{63}$$

Considering the operations of the matrix traces and $M=M^{\mathrm{T}}>0$, we can obtain

$$\begin{aligned}
&L(k)\Big(C\Big(\tilde{P}(k)+\sum_{i=1}^{h}(\tilde{P}_{1i}(k)+\tilde{P}_{2i}(k)+\tilde{P}_{3i}(k))\Big)C^{\mathrm{T}}+Q_v\Big)\\
&=A\Big(\tilde{P}(k)+\sum_{i=1}^{h}(\tilde{P}_{1i}(k)+\tilde{P}_{2i}(k)+\tilde{P}_{3i}(k))\Big)C^{\mathrm{T}}\\
&\quad+A_h\tilde{\hat{G}}(k-h)\tilde{\hat{G}}^{\mathrm{T}}(k-h)\Big(\prod_{i=1}^{h}(A-L(k-i)C)\Big)^{\mathrm{T}}C^{\mathrm{T}},
\end{aligned} \tag{64}$$

$$L(k)S(k)=AR_1(k)+A_hR_2(k). \tag{65}$$

Thus, the following can be concluded:

$$L(k) = AK_1(k) + A_hK_2(k), \tag{66}$$

$$K_1(k) = R_1(k)S^{-1}(k), \tag{67}$$

$$K_2(k) = R_2(k)S^{-1}(k), \tag{68}$$

$$R_1(k) = \big(\tilde{P}(k) + \sum_{i=1}^{h}(\tilde{P}_{1i}(k) + \tilde{P}_{2i}(k) + \tilde{P}_{3i}(k))\big)C^{\mathrm{T}}, \tag{69}$$

$$R_2(k) = A_h\tilde{\tilde{G}}(k-h)\tilde{\tilde{G}}^{\mathrm{T}}(k-h) \times \big(\prod_{i=1}^{h}(A - L(k-i)C)\big)^{\mathrm{T}}C^{\mathrm{T}}, \tag{70}$$

$$S(k) = C\big(\tilde{P}(k) + \sum_{i=1}^{h}(\tilde{P}_{1i}(k) + \tilde{P}_{2i}(k) + \tilde{P}_{3i}(k))\big)C^{\mathrm{T}} + Q_v, \tag{71}$$

$$\tilde{P}(k) = \big(\prod_{i=1}^{h}(A - L(k-i)C)\big)\tilde{\tilde{G}}(k-h)\tilde{\tilde{G}}^{\mathrm{T}}(k-h) \times \big(\prod_{i=1}^{h}(A - L(k-i)C)\big)^{\mathrm{T}}, \tag{72}$$

$$\tilde{P}_{1i}(k) = \big(\prod_{j=1}^{i-1}(A - L(k-j)C)\big)A_h\tilde{\tilde{G}}(k-h-i) \times \tilde{\tilde{G}}^{\mathrm{T}}(k-h-i)A_h^{\mathrm{T}}\big(\prod_{j=1}^{i-1}(A - L(k-j)C)\big)^{\mathrm{T}}, \tag{73}$$

$$\tilde{P}_{2i}(k) = \big(\prod_{j=1}^{i-1}(A - L(k-j)C)\big)DG_wG_w^{\mathrm{T}}D^{\mathrm{T}} \times \big(\prod_{j=1}^{i-1}(A - L(k-j)C)\big)^{\mathrm{T}}, \tag{74}$$

$$\tilde{P}_{3i}(k) = \big(\prod_{j=1}^{i-1}(A - L(k-j)C)\big)L(k-i)FG_vG_v^{\mathrm{T}}F^{\mathrm{T}} \times L^{\mathrm{T}}(k-i)\big(\prod_{j=1}^{i-1}(A - L(k-j)C)\big)^{\mathrm{T}},$$

$$Q_w = DG_wG_w^{\mathrm{T}}D^{\mathrm{T}}, \tag{75}$$

$$Q_v = FG_vG_v^{\mathrm{T}}F^{\mathrm{T}}. \tag{76}$$

□

Remark 1: In the derivations of Theorems 2 and 4, $S(k)$ is assumed to be reversible. If $S(k)$ is irreversible, then the pseudo-inverse of $S(k)$ can be used to replace the inverse of $S(k)$; that is, $K(k) = R(k)S^{+}(k)$ in Theorem 2 and $K_1(k) = R_1S^{+}(k)$, $K_2(k) = R_2S^{+}(k)$ in Theorem 4.

4. FAULT DIAGNOSIS

In this section, an accurate state estimation result is obtained by applying the optimal ZKF algorithm for the system with time delay, and the estimated state is then used for fault diagnosis, which is divided into the following two steps: fault detection and fault identification.

4.1. Fault detection

4.1.1 Fault-detection analysis

When the system is fault-free, the calculation rule of the estimated output set $\hat{Y}(k) = \langle \hat{p}_y(k), \hat{G}_y(k)\rangle$ that is consistent with state $\hat{x}(k)$ is as follows:

$$\begin{aligned}\hat{y}(k) &= C\hat{x}(k) + Fv(k)\\ &\in (C \odot \langle \hat{p}(k), \hat{G}(k)\rangle) \oplus (F \odot \langle 0, G_v\rangle)\\ &= \langle C\hat{p}(k), [C\hat{G}(k)\ FG_v]\rangle\\ &= \langle \hat{p}_y(k), \hat{G}_y(k)\rangle,\end{aligned} \tag{77}$$

where $\hat{p}_y(k) \in \mathbb{R}^{n_y}$ and $\hat{G}_y(k) \in \mathbb{R}^{n_y \times r_{\hat{G}_y}}$. Apparently, the value of $\hat{y}(k)$ cannot be determined owing to the unknown noise $v(k)$; however, the zonotopic set $\hat{Y}(k)$ containing $\hat{y}(k)$ can be obtained according to the aforementioned calculation rule. Based on the estimated output set $\hat{Y}(k)$, the upper bound $\hat{y}_u(k)$ and lower bound $\hat{y}_l(k)$ satisfy the followings:

$$\hat{y}_u(k) = \hat{p}_y(k) + \begin{bmatrix} \sum_{j=1}^{r_{\hat{G}_y}} |\hat{G}_{y1j}(k)| \\ \vdots \\ \sum_{j=1}^{r_{\hat{G}_y}} |\hat{G}_{yn_yj}(k)| \end{bmatrix}, \tag{78}$$

$$\hat{y}_l(k) = \hat{p}_y(k) - \begin{bmatrix} \sum_{j=1}^{r_{\hat{G}_y}} |\hat{G}_{y1j}(k)| \\ \vdots \\ \sum_{j=1}^{r_{\hat{G}_y}} |\hat{G}_{yn_yj}(k)| \end{bmatrix}. \tag{79}$$

If the true output value $y_t(k)$ satisfies $\hat{y}_{l1}(k) \le y_{t1}(k) \le \hat{y}_{u1}(k), \cdots, \hat{y}_{ln_y}(k) \le y_{tn_y}(k) \le \hat{y}_{un_y}(k)$, then it is determined that $y_t(k) \in \hat{Y}(k)$; otherwise, $y_t(k) \notin \hat{Y}(k)$. When a parameter fault occurs in the system, it leads to $y_t(k) \notin \hat{Y}(k)$, which indicates that there must be a fault in the system. $f(k)$ is defined as the fault-detection signal; it is $f(k) = 0$ when $y_t(k) \in \hat{Y}(k)$ and is $f(k) = 1$ when $y_t(k) \notin \hat{Y}(k)$, indicating the system is fault-free and faulty, respectively. To facilitate the development of this study, it is assumed that only one fault at a time occurs in the system, and the system parameters do not change over a certain period of time.

4.1.2 False alarm rate analysis

The fault-detection method based on the optimal ZKF is completed by detecting whether the true output value of the system is within the upper and lower bounds of the estimated output. The judgment criterion of fault detection can be expressed as follows: when the true output

value is not within the upper and lower bounds of the estimated output, the system is determined to be faulty; otherwise, the system is determined to be fault-free. The fault-detection strategy is based on the fact that in each iteration, the upper and lower bounds of the estimated output of the system are determined by the corresponding zonotopic set $\hat{Y}(k)$. When there is no fault in the system, the true output of the system must be included in the zonotopic set $\hat{Y}(k)$; that is, it is also included in the corresponding upper and lower bounds of $\hat{Y}(k)$. If the true output value is not within the upper and lower bounds of the estimated output, the system will fail. Therefore, given the noise boundaries, the fault-detection method based on the optimal ZKF proposed in this study will not cause a false alarm, that is, the false alarm rate is zero. Namely, once a fault alarm occurs, it indicates that there must be a fault in the system.

4.2. Fault identification

The error between the estimated and true states of the ith fault at each time k can be calculated using (80) as follows:

$$e_i(k) = \|\hat{p}(k) - p_{i,0}(k)\| / \|p_{i,0}(k)\|, \quad (i = 1,\ 2,\ \cdots,\ q), \tag{80}$$

where q is the number of parameter fault types in the fault library, $p_{i,0}(k)$ is the fault state of the ith fault type in the fault library. The continuous-time length L is selected, and the number of estimated errors that satisfy $e_i(k-l) < \varepsilon(k)$, $(l = 1, 2, \cdots, L)$ can be counted as $l_i(k)$, $(i = 1, 2, \cdots, q)$, where $\varepsilon(k)$ is the selected threshold. The value of $\varepsilon(k)$ is relative, and it is related to the practical system and the requirements of computational load. In the practical system, the value of each fault type of each system is different, so the demand for $\varepsilon(k)$ is different when distinguishing the fault types of systems. In the aspect of the requirements of computational load, the value of $\varepsilon(k)$ directly determines the amount of calculation required to identify system faults. If it is necessary to complete the fault identification as soon as possible with a small computational load, the value of $\varepsilon(k)$ can be increased appropriately. If none of the estimated states satisfy $e_i(k-l) < \varepsilon(k)$, $(l = 1, 2, \cdots, L, i = 1, 2, \cdots, q)$, a new fault outside the fault library at time k can be considered to have occurred, which is denoted as fault f_{q+1}. The number of new faults is counted at this moment and is recorded as $l_{q+1}(k)$.

The posterior probability of each fault type in the fault library was calculated and recorded as $P_i(k)$. Considering the possible new fault types, there are $q+1$ fault types. At the initial moment, the prior probability of each fault type is the same, which is $P_i(1) = 1/(q+1)$, $(i = 1, 2, \cdots, q+1)$. The posterior probability $P_i(k)$, whose fault type is fault f_i, $(i = 1, 2, \cdots, q+1)$, can then be calculated using (81) as follows:

$$P_i(k) = \frac{P_i(k-1)l_i(k)}{\sum_{j=1}^{q+1} P_j(k-1)l_j(k)}. \tag{81}$$

When the posterior probability satisfies (82), the fault diagnosis is complete; that is, if the posterior probability $P_i(k)$ satisfies (82), the fault is recognized as f_i

$$P_i(k) \geq 1 - \varsigma, \tag{82}$$

where ς is the set recognition accuracy.

5. SIMULATION ANALYSIS

5.1. Simulation 1: Numerical simulation

Consider the following linear discrete uncertain system with time delay:

$$\begin{cases} x(k+1) = Ax(k) + A_h x(k-h) + Bu(k) + Dw(k), \\ y(k) = Cx(k) + Fv(k), \end{cases} \tag{83}$$

where

$$A = \begin{bmatrix} 0.6 & -0.4 \\ -0.5 & 0.2 \end{bmatrix},\ A_h = \begin{bmatrix} -0.05 & -0.03 \\ 0.04 & -0.03 \end{bmatrix},$$
$$B = \begin{bmatrix} 0.2 \\ 0.2 \end{bmatrix},\ D = \begin{bmatrix} -0.1 \\ 0.1 \end{bmatrix},\ C = \begin{bmatrix} 1 & 0 \\ 0 & 1 \end{bmatrix},$$
$$F = \begin{bmatrix} 1 & 0 \\ 0 & 1 \end{bmatrix},\ h = 5.$$

$u(k) = 6$ is selected as the known input; the initial state, measurement noise, and process interference of the system are assumed to meet respectively as follows:

$$x(k-h) \in X(k-h) = \left\langle \begin{bmatrix} 2 \\ 3 \end{bmatrix},\ \begin{bmatrix} 2 & 0 \\ 0 & 2 \end{bmatrix} \right\rangle, \quad 0 \leqslant k \leqslant h, \tag{84}$$

$$w(k) \in W = \langle 0,\ 0.1 \rangle,\ k \geqslant 0, \tag{85}$$

$$v(k) \in V = \left\langle \begin{bmatrix} 0 \\ 0 \end{bmatrix},\ \begin{bmatrix} 0.1 & 0 \\ 0 & 0.1 \end{bmatrix} \right\rangle,\ k \geqslant 0. \tag{86}$$

Next, in this numerical case, the fault-diagnosis algorithm is analyzed in the following two situations: fault-free, and faulty in the fault library.

5.1.1 Fault-free

When the system is fault-free, Fig. 1 shows that the states can be estimated effectively by the designed optimal ZKF algorithm for the system with time delay, and the estimated state and true state are all within the upper and lower bounds of the estimated state. Fig. 2 illustrates that although there are small fluctuations in the true output values of the system, they are within the upper and lower bounds of the estimated output values. The upper and lower bounds of the estimated state and output fluctuate and converge to a certain extent in the initial time

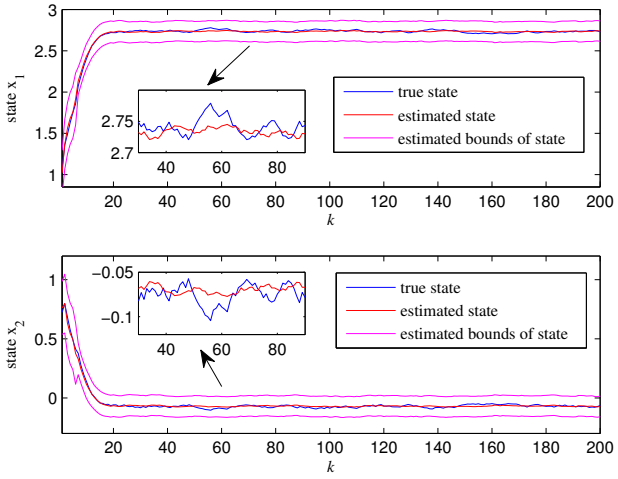

Fig. 1. Bounds of estimated states in a fault-free state.

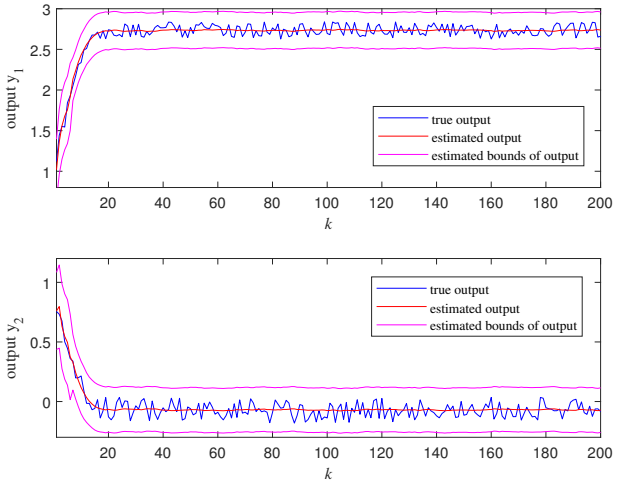

Fig. 2. Bounds of estimated outputs in a fault-free state.

period and remain unchanged after the system is stable. Thus, we can conclude that the system is fault-free, and the optimal ZKF method proposed in this study is effective and feasible for the state estimation of the system with time delay.

5.1.2 Fault in the fault library

Assuming that the system fault is caused by the parameter matrix A, and there are three types of faults in the fault library of the numerical system with time delay, the specific parameter changes are as follows: $A_1 = \begin{bmatrix} 0.6 & -0.4 \\ -0.4 & 0.2 \end{bmatrix}$, $A_2 = \begin{bmatrix} 0.6 & -0.4 \\ -0.4 & 0.5 \end{bmatrix}$, and $A_3 = \begin{bmatrix} 0.4 & -0.4 \\ -0.4 & 0.2 \end{bmatrix}$, and the corresponding faults are f_1, f_2, and f_3, respectively. The filters $fl_1 \sim fl_4$ corresponding to faults $f_1 \sim f_4$ are provided to indicate the types of faults identified, and f_4 represents the new fault outside the fault library. In this faulty state, fault f_1 is added to

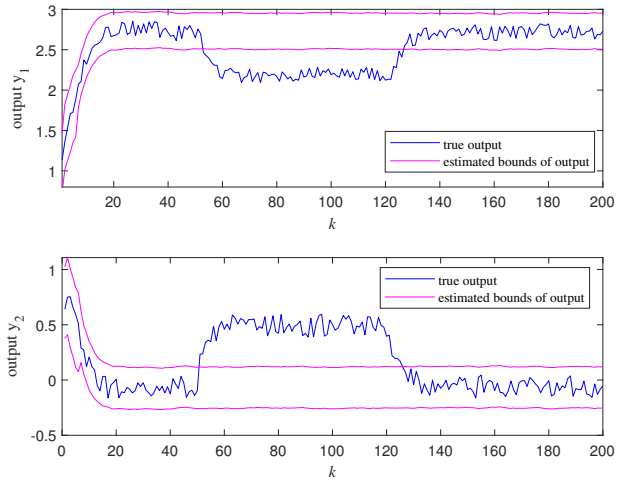

Fig. 3. True output in the scenario of fault in the fault library and the estimated bounds of y.

the system during the time period $k \in \{50, 120\}$. Considering the effect of historical data during the fault period, the difference between the true and fault states in the fault library was large in the beginning, and subsequently decreased rapidly and was maintained within a certain small range. Therefore, the value of $\varepsilon(k)$ should be set dynamically; specifically, the value of $\varepsilon(k)$ changes from 1.2 to 0.1 within ten-time points after the fault-detection point, and then remains unchanged at 0.1 in the subsequent fault identification process. For $\varsigma = 0.3$ and $L = 5$, the fault-diagnosis results are shown in Figs. 3-6.

As shown in Fig. 3, the true output values of the system are within the upper and lower bounds of the output values estimated by the optimal ZKF algorithm at the beginning, indicating that the system is in a normal state. The true output values of the system began to change and went beyond the upper and lower bounds of the output values estimated by the optimal ZKF algorithm at approximately $k = 50$, indicating that the system has a fault at that moment; hence, the zonotopic set of the output estimated by the optimal ZKF algorithm no longer contains the true output value. The true output values of the system return to be within the upper and lower bounds of the output values estimated by the optimal ZKF algorithm at approximately $k = 120$, indicating that the system returns to the normal from the fault state at this time, and the system only has a fault between $k = 50 \sim 120$ during the entire operating process.

Fig. 4 presents the relationship between the true output and the estimated zonotopic set more intuitively; the normal time period before the fault, the faulty time period during the fault, and the normal time period after the fault are selected as the representative time periods, considering one point, two points, and one point in the three representative time periods as examples, respectively. The

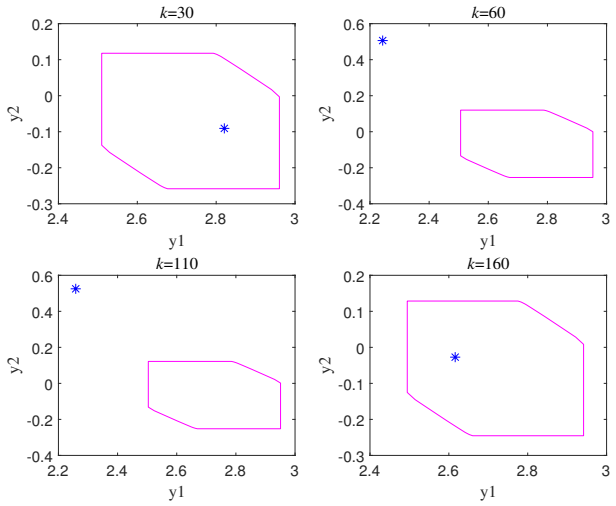

Fig. 4. True output in the scenario of fault in fault library and the estimated output at different times.

magenta zonotope is the approximate feasible set of the output estimated by the optimal ZKF algorithm, and the blue star indicates the true output value of the system. As indicated by Fig. 4, when $k = 60$ and $k = 110$, the system is in a fault state, and the zonotopic sets of output y estimated by the optimal ZKF algorithm do not contain the true output values of the system with the time delay at the fault time. Moreover, when the system is in a normal state, at times $k = 30$ and $k = 160$, the zonotopic sets estimated by the optimal ZKF algorithm contain the true outputs of the system, indicating that the detection result is consistent with the real system.

To obtain a more specific fault-occurrence time, the curve of the fault-detection signal f is shown in Fig. 5; it indicates that the system is detected to have a fault during time $k = 50 \sim 127$ by the proposed fault-detection algorithm, which is close to the real fault time when slight delays are ignored. Subsequently, the algorithm enters the fault identification stage; $fp_1 \sim fp_4$ represents the fault-matching probability of $f_1 \sim f_4$. Because the fault that occurred in the system was set as fault f_1 in the fault library, the fault-matching probability of the three faults in the fault library correspondingly increases in the initial stage of fault identification. According to the judgment rule of the new fault f_4 for fault identification, fp_4 will soon decrease to 0 among the four fault-matching probability curves, which also indicates that the probability of a new fault occurring in the system is minimal. Thereafter, fp_2 and fp_3 begin to gradually decrease to 0 after a short period of rise, whereas fp_1 increases gradually and eventually remains at 1. When the matching probability is not less than $1 - \varsigma$, the corresponding fault identification filter fl_1 spikes at $k = 53$, indicating that the fault type of the system is f_1.

A normal fault-matching method is compared to the

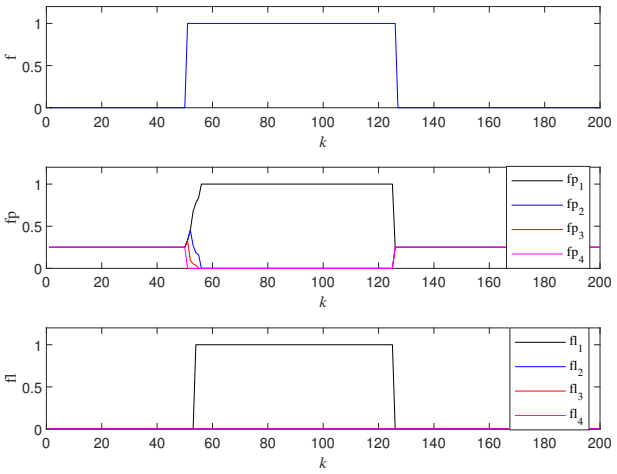

Fig. 5. Fault diagnosis results in the scenario of fault in the fault library.

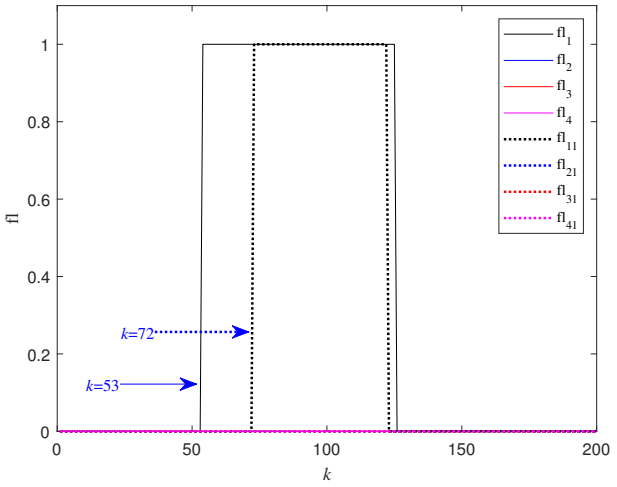

Fig. 6. Comparison of fault identification results of the two algorithms for scenarios of fault in the fault library.

proposed fault-diagnosis algorithm to further demonstrate its advantages. The normal fault-matching method separates the fault by making the error between the estimated and true states of the ith fault less than a fixed threshold $\varepsilon'(k)$ in a continuous period L'. The comparison curves of the fault identification obtained by the two algorithms are shown in Fig. 6. In this simulation, L' and $\varepsilon'(k)$ were set to 20 and 0.1, respectively. $fl_1 \sim fl_4$ in Fig. 6 are the fault-diagnosis filters corresponding to $f_1 \sim f_4$ using the fault-diagnosis algorithm combining the fault-matching method and Bayesian theory, and $fl_{11} \sim fl_{41}$ indicate the fault identification results corresponding to $f_1 \sim f_4$ through the normal fault-matching algorithm. According to the figure, the normal fault-matching algorithm can identify the fault type of the pitch system; however, fault identification is achieved at $k = 72$, which is 19 time points slower than

the proposed algorithm, indicating that its fault identification speed is significantly slower than that of the fault-diagnosis algorithm proposed in this study.

5.2. Simulation 2: Pitch system of wind turbine

Wind turbines are prone to failure in the process of power generation, and several scholars have studied the corresponding fault diagnosis [36]. As shown in Fig. 7, the pitch system is an important part of the blade control and pitch angle conversion of a wind turbine.

The mathematical model of the pitch system can be expressed as follows [37]:

$$\begin{bmatrix}\dot{\beta}\\ \dot{\beta}_a\end{bmatrix}=\begin{bmatrix}0 & 1\\ -\omega_n^2 & -2\zeta\omega_n\end{bmatrix}\begin{bmatrix}\beta\\ \beta_a\end{bmatrix}+\begin{bmatrix}0\\ \omega_n^2\end{bmatrix}\beta_r, \tag{87}$$

where β and β_a are the pitch angle and angular velocity, respectively; β_r is the reference value of the pitch, and ω_n and ζ are the system parameters. Let $\omega_n = 11.11$ rad/s and $\zeta = 0.6$ be the natural frequency and damping coefficient of the system, respectively. The system can be expressed as a continuous-time state-space equation as follows:

$$\dot{x}=\begin{bmatrix}0 & 1\\ -\omega_n^2 & -2\zeta\omega_n\end{bmatrix}x+\begin{bmatrix}0\\ \omega_n^2\end{bmatrix}u+\begin{bmatrix}0 & 0\\ -\frac{\omega_n^2}{2} & -\frac{\omega_n^2}{2}\end{bmatrix}w, \tag{88}$$

$$y=Cx+Fv, \tag{89}$$

where $x=[\beta\ \beta_a]^T$, $u=\beta_r$, and w and v are the interference and output noise, respectively. Let the sampling time be $T_s = 0.01$ s, the system is discretized, where

$$A=\begin{bmatrix}0.9941 & 0.0093\\ -1.1532 & 0.8695\end{bmatrix},\ B=\begin{bmatrix}0.0059\\ 1.1532\end{bmatrix},$$
$$F=\begin{bmatrix}1 & 0\\ 0 & 1\end{bmatrix},\ D=\begin{bmatrix}-0.0030 & -0.0030\\ -0.5766 & -0.5766\end{bmatrix},$$
$$C=\begin{bmatrix}1 & 0\\ 0.5 & 0.1\end{bmatrix}.$$

We consider the influence of the time delay of the state on the pitch system, and select $A_h=\begin{bmatrix}-0.005 & -0.003\\ 0.004 & -0.003\end{bmatrix}$, $h=$ 6. The sinusoidal signal $u(k)=1.5\sin(6k)+7$ is selected as the external excitation signal, and it is assumed that the initial state, process interference, and measurement noise of the system meet, respectively, as follows:

$$x(k-h)\in X(k-h)=\left\langle\begin{bmatrix}6.5\\ 0\end{bmatrix},\begin{bmatrix}5 & 0\\ 0 & 5\end{bmatrix}\right\rangle,\quad 0\leqslant k\leqslant h, \tag{90}$$

$$w(k)\in W=\left\langle\begin{bmatrix}0\\ 0\end{bmatrix},\begin{bmatrix}0.1 & 0\\ 0 & 0.1\end{bmatrix}\right\rangle,\ k\geqslant 0, \tag{91}$$

$$v(k)\in V=\left\langle\begin{bmatrix}0\\ 0\end{bmatrix},\begin{bmatrix}0.1 & 0\\ 0 & 0.1\end{bmatrix}\right\rangle,\ k\geqslant 0. \tag{92}$$

Subsequently, in this pitch system case, the fault-diagnosis algorithm is analyzed in the following two situations: fault-free, and fault outside the fault library.

5.2.1 Fault-free

As shown in Fig. 8, when the pitch system is fault-free, the optimal ZKF algorithm proposed in this study for a linear system with time delay has a sufficient state estimation performance. The estimated state curve rapidly follows the true state of the system; the two curves are included in the upper and lower bounds of the estimated state. As shown in Fig. 9, the true output value of the system is within the upper and lower bounds of the output value estimated by the optimal ZKF algorithm when the pitch system is fault-free.

5.2.2 Fault outside the fault library

The following three faults are in the fault library of the pitch system [38]: pressure drop, pump wear, and air content increase, which are defined as faults f_1, f_2, and f_3, respectively. The new fault outside the fault library is defined as fault f_4. The faulty parameter values are listed in Table 1.

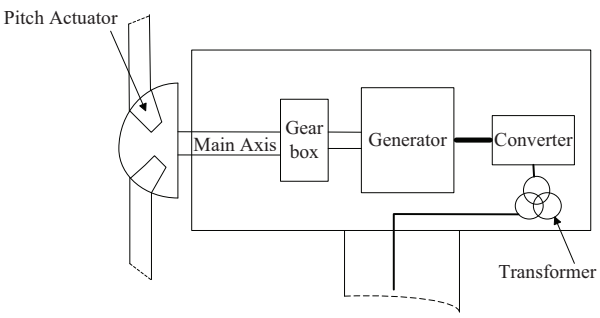

Fig. 7. Wind turbine system.

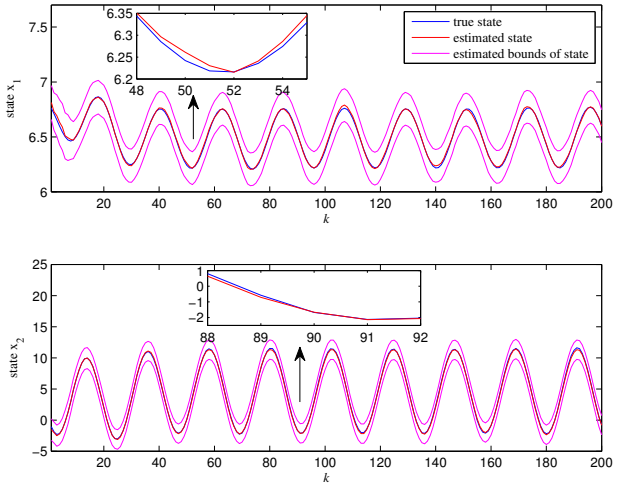

Fig. 8. Bounds of x in a fault-free state.

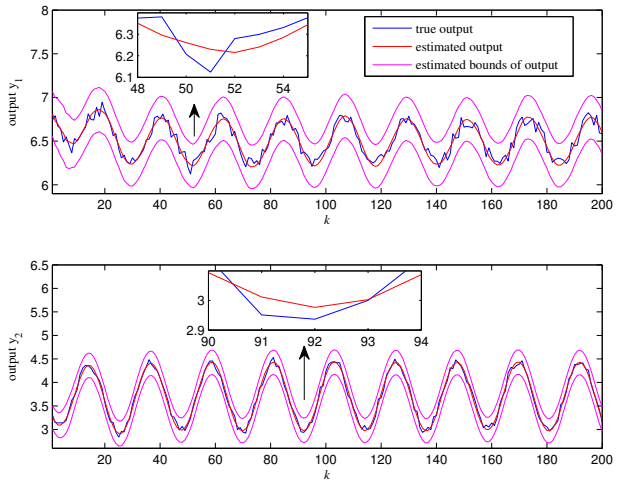

Fig. 9. Bounds of y in a fault-free state.

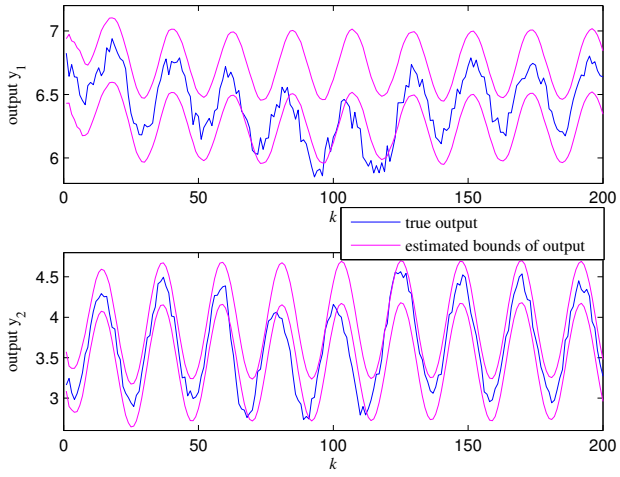

Fig. 10. True output in the scenario of fault outside the fault library and bounds of y.

Table 1. Parameters of pitch system in fault conditions.

	Fault	Parameters
f_1	Pressure drop	$\xi_1 = 0.45$, $\omega_{n1} = 5.73$ rad/s
f_2	Pump wear	$\xi_2 = 0.75$, $\omega_{n2} = 7.27$ rad/s
f_3	Air content increase	$\xi_3 = 0.90$, $\omega_{n3} = 3.42$ rad/s
f_4	New fault	$\xi_4 = 1.60$, $\omega_{n4} = 15.00$ rad/s

Given the actual system, we assume that the types of faults that may occur in the actual system are those faults in the fault library and the new fault outside the fault library when $60 \leqslant k \leqslant 115$, which are defined as $f_1 \sim f_4$; filters corresponding to faults $f_1 \sim f_4$ are provided to indicate the types of faults identified. In this scenario, f_4 is included in (88) when $60 \leqslant k \leqslant 115$. Figs. 10-13 show the fault diagnosis results of the proposed fault-diagnosis algorithm, and Fig. 13 presents the comparison results of the fault identification using the proposed algorithm and the normal fault-matching algorithm.

Fig. 10 indicates that the true output values of the pitch system begin to go beyond the upper and lower bounds of the output values estimated by the optimal ZKF algorithm at approximately $k = 60$, and return to be within the bounds at approximately $k = 120$, indicating that the system fault occurs and ends at approximately $k = 60$ and $k = 120$, respectively; thereafter, the system resumes normal operation. The output values estimated by the optimal ZKF algorithm at different time points in Fig. 11 verify the correctness of the proposed algorithm more specifically. When $k = 30$ and $k = 160$, the zonotopic sets of the output values estimated by the optimal ZKF algorithm (magenta lines) all contain the true output values (blue stars), while the zonotopic sets of the output values do not contain the true output values when $k = 80$ and $k = 110$, which is consistent with the fault state of the real pitch system.

The curve of the fault-detection signal f is shown in

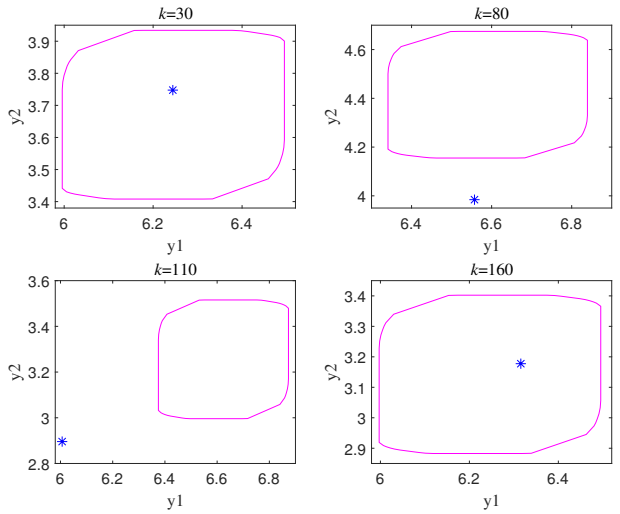

Fig. 11. True output in the scenario of a fault outside the fault library and the estimated output at different times.

Fig. 12, indicating that the specific time of the faults detected by the fault-diagnosis algorithm is $k \in \{61 \sim 124\}$, which is close to the real time of the system fault, thus we can conclude that the proposed algorithm has a sufficient fault-detection performance.

Set $\varsigma = 0.3$, $L = 8$, and $\varepsilon(k)$ changes dynamically during the fault period and its value decreases from 0.2 to 0.1 within 10 time points after the fault-detection point, and then remains at 0.1 until the end of the fault. As shown in Fig. 12, the fault-matching probability fp_4 gradually increases to 1 during the fault period. When fp_4 is greater than $1 - \varsigma$, the corresponding fault identification filter fl_4 is set to be 1 at time $k = 64$, which indicates that during the entire working period of the pitch system, the new fault f_4 outside the fault library occurs after a period of normal

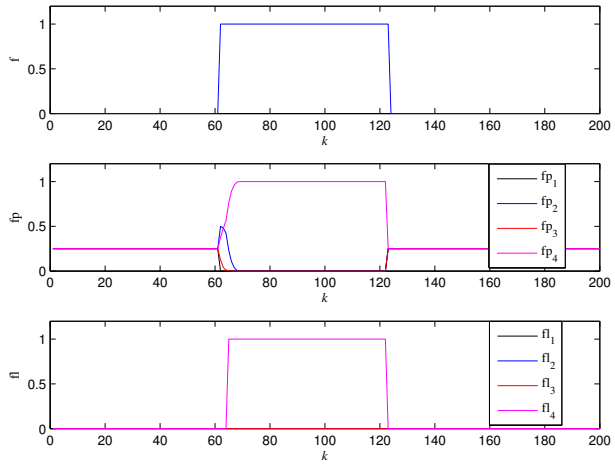

Fig. 12. Fault diagnosis results in the scenario of fault outside the fault library.

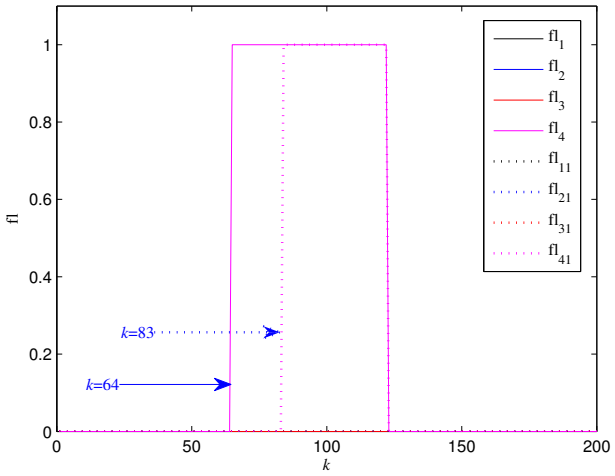

Fig. 13. Comparison of fault identification results of the two algorithms in the scenario of a fault outside the fault library.

state.

As shown in Fig. 13, the comparison curves between the two algorithms show that the fault identification time of the fault-diagnosis algorithm based on the combination of the fault-matching method and Bayesian theory is 19 time points faster than that of the normal fault-matching algorithm. Thus, the proposed fault-diagnosis algorithm has an advantage in terms of the speed of fault identification.

6. CONCLUSION

In this study, a state estimation and fault-diagnosis method based on the optimal zonotopic Kalman filter is presented for a linear discrete-time system with time delay. The optimal observer gain of the optimal zonotopic Kalman filter was designed by minimizing the size of the zonotopic set to estimate the state set. The parameter fault-diagnosis problems of a numerical system and the pitch system of a wind turbine are used as examples to verify the effectiveness and feasibility of the algorithm.

The fault-diagnosis method proposed in this study can also be applied to combine certain parameter estimation algorithms [39,40] to study the fault-diagnosis problems of other time-delay industrial processes with unknown but bounded noise. In addition, based on the proposed fault-diagnosis algorithm, the study can be further extended to the fault diagnosis of other complex systems, such as Markovian systems [41,42] and applications [43].

REFERENCES

[1] C. Edwards and S. Simani, "Fault diagnosis and fault-tolerant control in aerospace systems," *International Journal of Robust and Nonlinear Control*, vol. 29, no. 16, pp. 5291-5292, November 2019.

[2] Q. H. Zhang, "Adaptive Kalman filter for actuator fault diagnosis," *Automatica*, vol. 93, pp. 333-342, July 2018.

[3] Y. J. Wang, J. Q. Tian, Z. H, Chen, and X. T. Liu, "Model based insulation fault diagnosis for lithium-ion battery pack in electric vehicles," *Measurement*, vol. 131, pp. 443-451, January 2019.

[4] Y. Zhao and Y. Shen, "Distributed event-triggered state estimation and fault detection of nonlinear stochastic systems" *Journal of the Franklin Institute-Engineering and Applied Mathematics*, vol. 356, no. 17, pp. 10335-10354, November 2019.

[5] H. R. Hwang, B. S. Kim, T. H. Cho, and I. S. Lee, "Implementation of a fault diagnosis system using neural networks for solar panel," *International Journal of Control, Automation, and Systems*, vol. 17, no. 4, pp. 1050-1058, April 2019.

[6] K. Verbert, R. Babuska, and B. De Schutter, "Bayesian and Dempster-Shafer reasoning for knowledge-based fault diagnosis-A comparative study," *Engineering Applications of Artificial Intelligence*, vol. 60, pp. 136-150, April 2017.

[7] H. Talhaoui, A. Menacer, A. Kessal, and A. Tarek, "Experimental diagnosis of broken rotor bars fault in induction machine based on Hilbert and discrete wavelet transforms," *International Journal of Advanced Manufacturing Technology*, vol. 95, no. 1-4, pp. 1399-1408, March 2018.

[8] N. T. Truong, T. I. Seo, and S. D. Nguyen, "Bearing fault online identification based on ANFIS," *International Journal of Control, Automation, and Systems*, vol. 19, no. 4, pp. 1703-1714, April 2021.

[9] J. Y. Gong, B. Jiang, and Q. K. Shen, "Distributed-observer-based fault tolerant control design for nonlinear multi-agent systems" *International Journal of Control, Automation, and Systems*, vol. 17, no. 12, pp. 3149-3157, December 2019.

[10] Q. K. Shen, B. Jiang, and P. Shi, "Adaptive fault tolerant control against actuator faults" *International Journal of Adaptive Control and Signal Processing*, vol. 31, no. 2, pp. 147-162, February 2017.

[11] R. Khan, P. Williams, P. Riseborough, A. Rao, and R. Hill, "Fault detection and identification-A filter investigation," *International Journal of Robust and Nonlinear Control*, vol. 28, no. 5, pp. 1852-1870, March 2018.

[12] F. Naseri, H. Samet, T. Ghanbari, and E. Farjah, "Power transformer differential protection based on least squares algorithm with extended kernel," *IET Science Measurement & Technology*, vol. 13, no. 8, pp. 1102-1110, October 2019.

[13] N. D. Peric, R. Paulen, M. E. Villanueva, and B. Chachuat, "Set-membership nonlinear regression approach to parameter estimation," *IET Science Measurement & Technology*, vol. 70, pp. 80-95, October 2018.

[14] M. Casini, A. Garulli, and A. Vicino, "A linear programming approach to online set membership parameter estimation for linear regression models," *International Journal of Adaptive Control and Signal Processing*, vol. 31, no. 3, pp. 360-378, March 2017.

[15] Y. Wang, Z. H. Wang, V. Puig, and G. Cembrano, "Zonotopic set-membership state estimation for discrete-time descriptor LPV systems," *IEEE Transactions on Automatic Control*, vol. 64, no. 5, pp. 2092-2099, May 2019.

[16] M. Pourasghar, V. Puig, and C. Ocampo-Martinez, "Interval observer versus set-membership approaches for fault detection in uncertain systems using zonotopes," *International Journal of Advanced Manufacturing Technology*, vol. 29, no. 10, pp. 2819-2843, July 2019.

[17] M. Buciakowski, M. Witczak, V. Puig, D. Rotondo, F. Nejjari, and J. Korbicz, "A bounded-error approach to simultaneous state and actuator fault estimation for a class of nonlinear systems," *Journal of Process Control*, vol. 52, pp. 14-25, April 2017.

[18] J. Wang, J. D. Wang, and M. Zhou, "On-line auxiliary input signal design for active fault detection and isolation based on set-membership and moving window techniques," *International Journal of Control, Automation, and Systems*, vol. 17, no. 11, pp. 2796-2806, November 2019.

[19] D. Y. Chen, N. Yang, J. Hu, and J. H. Du, "Resilient set-membership state estimation for uncertain complex networks with sensor saturation under round-robin protocol," *International Journal of Control, Automation, and Systems*, vol. 17, no. 12, pp. 3035-3046, December 2019.

[20] J. T. Li, Z. H. Wang, Y. Shen, and M. Rodrigues, "Zonotopic fault detection observer for linear parameter-varying descriptor systems," *International Journal of Robust and Nonlinear Control*, vol. 29, no. 11, pp. 3426-3445, July 2019.

[21] D. Rotondo, F. Nejjari, V. Puig, and J. Blesa, "Model reference FTC for LPV systems using virtual actuators and set-membership fault estimation," *International Journal of Robust and Nonlinear Control*, vol. 25, no. 5, pp. 735-760, March 2015.

[22] J. C. Hu and B. C. Ding, "An efficient offline implementation for output feedback min-max MPC," *International Journal of Robust and Nonlinear Control*, vol. 29, no. 2, pp. 492-506, January 2018.

[23] V. T. H. Le, C. Stoica, T. Alamo, E. F. Camacho, and D. Dumur, "Zonotopic guaranteed state estimation for uncertain systems," *Automatica*, vol. 49, no. 11, pp. 3418-3424, November 2013.

[24] C. Combastel, "Zonotopes and Kalman observers: Gain optimality under distinct uncertainty paradigms and robust convergence," *Automatica*, vol. 55, pp. 265-273, May 2015.

[25] W. H. Zhang, Z. H. Wang, S. H. Guo, and Y. Shen, "Interval estimation of sensor fault based on zonotopic Kalman filter," *International Journal of Control*, vol. 94, no. 6, pp. 1641-1650, September 2019.

[26] M. Pourasghar, C. Combastel, V. Puig, and C. Ocampo-Martinez, "FD-ZKF: A zonotopic Kalman filter optimizing fault detection rather than state estimation," *Journal of Process Control*, vol. 73, pp. 89-102, January 2019.

[27] H. Y. Shi, P. Li, J. T. Cao, C. L. Su, and J. X. Yu, "Robust fuzzy predictive control for discrete-time systems with interval time-varying delays and unknown disturbances," *IEEE Transactions on Fuzzy Systems*, vol. 28, no. 7, pp. 1504-1516, July 2020.

[28] Y. Zhao, J. Wang, F. Yan, and Y. Shen, "Adaptive sliding mode fault-tolerant control for type-2 fuzzy systems with distributed delays" *Information Sciences*, vol. 473, pp. 227-238, January 2019.

[29] R. M. Yang, F. Y. Zang, L. Y. Sun, P. Zhou, and B. H. Zhang, "Finite-time adaptive robust control of nonlinear time-delay uncertain systems with disturbance," *International Journal of Robust and Nonlinear Control*, vol. 29, no. 4, pp. 919-934, March 2019.

[30] P. P. Yang, Y. Tang, M. D. Yan, and X. Zhu, "Consensus based control algorithm for nnonlinear vehicle platoons in the presence of time delay," *International Journal of Control, Automation, and Systems*, vol. 17, no. 3, pp. 752-764, March 2019.

[31] J. H. Yook, I. H. Kim, M. S. Han, and Y. I. Son, "Robustness improvement of DC motor speed control using communication disturbance observer under uncertain time delay," *Electronics Letters*, vol. 53, no. 6, pp. 389-391, March 2017.

[32] Z. H. Zhang, Z. H. Wang, W. T. Tang, Z. G. Feng, and Y. Shen, "Zonotopic reachable set estimation for linear discrete-time systems with time delay," *International Journal of Robust and Nonlinear Control*, vol. 30, no. 14, pp. 5542-5558, July 2020.

[33] F. Q. You, H. Li, Y. W. Zhang, and S. P. Guan, "A novel sensor fault diagnosis approach for time-varying delay systems with non-linear uncertainty," *Transactions of the Institute of Measurement and Control*, vol. 39, no. 7, pp. 1114-1120, July 2017.

[34] X. Y. Tong, W. C. Lian, and H. B. Wang, "A novel online multi-section weighed fault matching and detecting algorithm based on wide-area information," *Journal of Electrical Engineering & Technology*, vol. 12, no. 6, pp. 2118-2126, November 2017.

[35] Y. Wang, Z. H. Wang, V. Puig, and G. Cembrano, "Zonotopic fault estimation filter design for discrete-time descriptor systems," *IFAC-PapersOnLine*, vol. 50, no. 1, pp. 5055-5060, July 2017.

[36] L. I. Gliga, B. D. Ciubotaru, H. Chafouk, D. Popescu, and C. Lupu, "Fault diagnosis of a direct drive wind turbine using a bank of Goertzel filters," *Proc. of the 6th International Conference on Control, Decision and Information Technologies*, pp. 1729-1734, September 2019.

[37] M. Rahnavard, M. Ayati, M. R. H. Yazdi, and M. Mousavi, "Finite time estimation of actuator faults, states, and aerodynamic load of a realistic wind turbine," *Renewable Energy*, vol. 130, pp. 256-267, January 2019.

[38] D. H. Wu, W. Liu, J. Song, and Y. X. Shen, "Fault estimation and fault-tolerant control of wind turbines using the SDW-LSI algorithm," *IEEE Access*, vol. 4, pp. 7223-7231, 2016.

[39] L. Xu, W. L. Xiong, A. Alsaedi, and T. Hayat, "Hierarchical parameter estimation for the frequency response based on the dynamical window data," *International Journal of Control, Automation, and Systems*, vol. 16, no. 4, pp. 1756-1764, August 2018.

[40] Z. Y. Wang, Y. Wang, and Z. C. Ji, "A novel two-stage estimation algorithm for nonlinear Hammerstein-Wiener systems from noisy input and output data," *Journal of the Franklin Institute-Engineering and Applied Mathematics*, vol. 354, no. 4, pp. 1937-1944, March 2017.

[41] Y. Wang, H. Pu, P. Shi, C. K. Ahn, and J. Luo. "Sliding mode control for singularly perturbed Markov jump descriptor systems with nonlinear perturbation," *Automatica*, vol. 127, p. 109515, May 2021.

[42] J. Cheng, Y. Shan, J. Cao, J. H. Park, "Nonstationary control for T-S fuzzy Markovian switching systems with variable quantization density," *IEEE Transactions on Fuzzy Systems*, vol. 29, no. 6, pp. 1375-1385, June 2021.

[43] W. Zhou, J. Fu, H. Yan, X. Du, Y. Wang, and H. Zhou, "Event-triggered approximate optimal path-following control for unmanned surface vehicles with state constraints," *IEEE Transactions on Neural Networks and Learning Systems*, pp. 1-15, July 2021. DOI: 10.1109/TNNLS.2021.3090054

Zi-Xing Liu received her B.Sc. degree in automation from Jiangnan University, Jiangsu, China in 2019, and is currently pursuing an M.S. degree in Jiangnan University, Jiangsu, China. Her research interests include set-membership estimation and fault diagnosis.

Zi-Yun Wang received his B.Sc. degree in electronic information engineering from Jiangnan University in 2010 and a Ph.D. degree in control science and engineering from Jiangnan University in 2015. His research interests include system modeling and state estimation for practical industrial application.

Yan Wang received her Ph.D. degree in control science and engineering from Nanjing University of Science and Technology in 2006. Her research interests include system modeling and optimal scheduling.

Zhi-Cheng Ji received his Ph.D. degree in power electronics and power drives from China University of Mining and Technology in 2004. His research interests include nonlinear control, adaptive control, and system identification.